Oceanic basement roughness alongside magma-poor rifted margins: insight into initial seafloor spreading

Daniel Sauter, Julie Tugend, Morgane Gillard, Michael Nirrengarten, Julia Autin, Gianreto Manatschal, Mathilde Cannat, Sylvie Leroy, Marc Schaming

Geophysical Journal International

Geophys. J. Int. (2018) **212,** 900–915
Advance Access publication 2017 October 13
GJI Marine geosciences and applied geophysics

doi: 10.1093/gji/ggx439

Oceanic basement roughness alongside magma-poor rifted margins: insight into initial seafloor spreading

Daniel Sauter,[1] Julie Tugend,[1] Morgane Gillard,[1] Michael Nirrengarten,[1] Julia Autin,[1] Gianreto Manatschal,[1] Mathilde Cannat,[2] Sylvie Leroy[3] and Marc Schaming[1]

[1]*Institut de Physique du Globe de Strasbourg, CNRS UMR* 7516*, Université de Strasbourg,* 1 *rue Blessig, F-*67084 *Strasbourg Cedex, France. E-mail: daniel.sauter@unistra.fr*
[2]*Institut de Physique du Globe de Paris, CNRS UMR* 7154*,* 1 *rue Jussieu, F-*75238 *Paris Cedex* 05*, France*
[3]*Institut des Sciences de la Terre de Paris, CNRS UMR* 7193*, Sorbonne Universités, UPMC,* 4 *place Jussieu, F-*75252 *Paris Cedex* 05*, France*

Accepted 2017 October 12. Received 2017 September 8; in original form 2017 April 5

SUMMARY

The variation of oceanic basement roughness at mid-oceanic ridges is a complex trade-off between spreading rate that largely controls the thermal state of the lithosphere and its composition controlling the rheology and thus also the strength of the lithosphere. Here we estimate top basement roughness (i.e. the root-mean-square deviation of residual basement relief) over initial oceanic crust bordering the Iberia, Newfoundland, Bay of Biscay, Goban Spur, Flemish Cap, Australian and Antarctic rifted margins to provide new insights into the spreading processes at the nascent plate boundary. Although ultraslow seafloor spreading is suggested in those areas, the lack of undisputable oceanic magnetic anomalies prevents any well-constrained determination of the initial spreading rates. We compare these estimated roughness values with those determined over ultraslow-spreading crust formed at the Mid Atlantic Ridge, Southwest Indian Ridge, Arctic ridges, Mid-Cayman Spreading Center, Sheba ridge and South Pandora Ridge. The roughness values obtained at these ultraslow-spreading ridges range from 100 to >500 m and include 200–240 m roughness values which are typical of slow-spreading ridges. Roughness values larger than ∼300 m are characteristic of magma-poor sections of ultraslow-spreading ridges. The top basement roughness values determined within the inferred initial oceanic domain bordering the investigated magma-poor rifted margins are all higher than 200 m. Mean roughness values of the inferred initial oceanic domains alongside the conjugate Iberia and Newfoundland margins are greater than 300 m similarly to magma-poor sections of ultraslow-spreading ridges. The top basement in the initial oceanic crust alongside the conjugate Flemish Cap and Goban Spur margins shows roughness values and a tilted block morphology typical of slow-spreading ridges. We suggest that the roughness and the morphology of the top basement bordering the conjugate Australian and Antarctic margins indicate large tectonic extension and intermediate magma supply at either slow- or ultraslow-spreading rates. We show that estimating roughness values within transitional domains of magma-poor margins like exhumed mantle domains is less pertinent as polyphased tectonism and magmatism may have affected these domains leading to highly variable top basement roughness values that cannot be linked to a single process.

Key words: Composition and structure of the oceanic crust; Atlantic Ocean; Indian Ocean; Continental margins: divergent; Mid-ocean ridge processes; Submarine tectonics and volcanism.

1 INTRODUCTION

Up to recently, hydrocarbon exploration has influenced our knowledge of the formation of rifted margins by collecting data mainly over sedimentary basins proximal to the continent. The acquisition of oceanward seismic data combined with deep sea drilling at magma-poor rifted margins, particularly along the conjugate Iberia and Newfoundland margins, revealed that the proximal and distal domains are very different from each other. The discovery of hyperextended continental crust and exhumed subcontinental mantle in these conjugated margins led to debated models for crustal thinning (e.g. Ranero & Perez-Gussinye 2010; Sutra & Manatschal

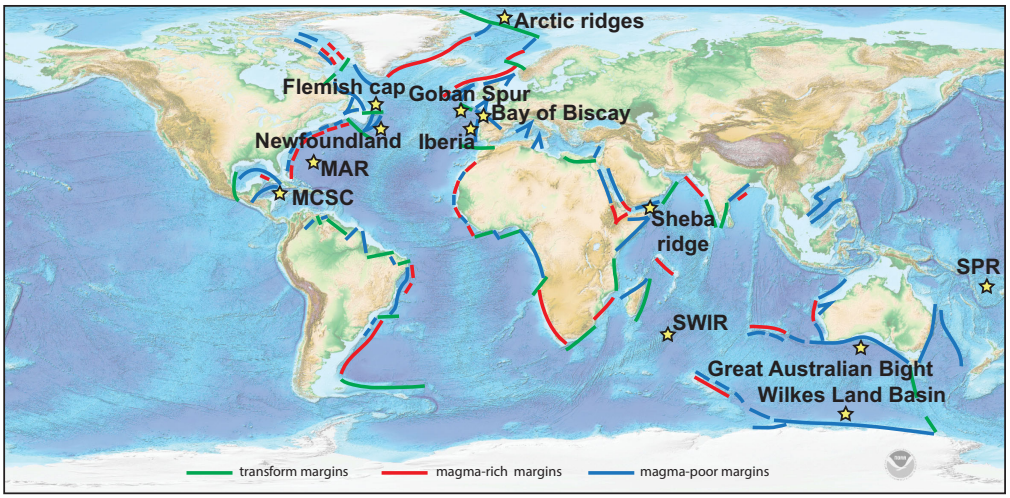

Figure 1. Worldwide distribution of the magma-poor rifted margin systems and locations of the rifted margins and mid-oceanic ridges discussed in this paper. MAR: Mid-Atlantic Ridge; MCSC: Mid Cayman Spreading Center; SPR: South Pandora Ridge; SWIR: Southwest Indian Ridge. After Haupert *et al.* (2016). Background image is from Amante & Eakins (2009).

2012; McDermott & Reston 2015). However, acquisition of both seismic and potential field data still remains, with some exceptions, focused to the rifted margin and only few lines image the transition to unambiguous oceanic crust. As a consequence, the transition to ocean crust is still poorly constrained. Terms like initial or incipient (Hopper *et al.* 2004), embryonic (Jagoutz *et al.* 2007) or proto-oceanic crust (Gillard *et al.* 2015) have been used to describe this transitional domain lacking clear geophysical characteristics of ocean crust like a well-marked reflector interpreted as the oceanic Moho on multichannel seismic (MCS) reflection data or typical velocity gradients on refraction data (Min 2009). Moreover, the lack of undisputable oceanic magnetic anomalies often did not allow the determination of initial spreading rates either because the onset of seafloor spreading fell within the Cretaceous Normal Superchron or because the ill-defined magnetic lineations may not be due to reversals of the Earth's magnetic field but to other processes (Bronner *et al.* 2011). However, occurrence of crust thinner (<5 km) than typical oceanic crust was thought to indicate that this transitional crust was emplaced at an ultraslow-spreading ridge (Hopper *et al.* 2004; van Avendonk *et al.* 2006).

Indeed, evidence for thin oceanic crust (<5 km) has been found at ultraslow-spreading ridges in the early 80s (Reid & Jackson 1981). This led to the suggestion that below a critical spreading rate (15–20 mm yr^{-1}), the melt supply per increment of plate separation is dramatically decreasing (Reid & Jackson 1981). This is thought to result from a thickening of the thermal boundary layer at those ridges which in turn reduces the height of the melting regime (White *et al.* 2001). In the last two decades exhumed mantle derived rocks have been found in wide areas of the ultraslow-spreading Southwest Indian Ridge (SWIR; Cannat *et al.* 2006; Sauter *et al.* 2013) and the Gakkel Ridge (Michael *et al.* 2003) and seismic data have shown thin crust in magma-poor sections of these ridges (Muller *et al.* 1999; Jokat *et al.* 2003; Minshull *et al.* 2006). However, very thick crust (8–10 km) has been recently discovered (Zhao *et al.* 2013; Li *et al.* 2015; Niu *et al.* 2015) at the shallowest part of a >550 km long thick crust ridge section of the SWIR (Sauter *et al.* 2009). Such along-axis large crustal thickness variations, while the ultraslow-spreading rate varies only slightly, are therefore challenging the current view of thin crust being associated with ultraslow spreading (Michael *et al.* 2003; Cannat *et al.* 2008).

It is commonly inferred that seafloor roughness (i.e. the root mean square deviation of residual basement relief) increases dramatically for full spreading rates of <40 mm yr^{-1} (Malinverno 1991; Ehlers & Jokat 2009). Top basement roughness could thus be used to identify ultraslow-spreading lithosphere. We therefore suggest that investigating the top basement roughness of initial oceanic domains bordering magma-poor rifted margins may provide new insights in the spreading processes triggered by lithospheric breakup. In this paper, we first review seafloor roughness estimates at present day ultraslow-spreading ridges based on published data from the SWIR and from the Arctic ridges and on new roughness estimations at the Mid-Cayman Spreading Center (MCSC), the Sheba ridge and at the South Pandora Ridge (SPR) in the North Fiji Basin (Fig. 1). We also investigate the relief on flanks of the Mid Atlantic Ridge (MAR), which were created when this ridge underwent ultraslow spreading. Results from measurements of the top basement roughness along MCS profiles on inferred initial oceanic domains bordering the Iberia, Newfoundland, Bay of Biscay (BB), Goban Spur (GS), Flemish Cap, Australian and Antarctic margins are then presented in a second part (Fig. 1). These top basement roughness values are compared to those of ultraslow-spreading ridges. We discuss how estimating the roughness of the top basement may help to constrain the spreading processes at the initial oceanic ridge. We found that roughness values of the inferred initial oceanic domains alongside the conjugate Iberia and Newfoundland margins are similar to those of magma-poor sections on ultraslow-spreading ridges. In contrast, the top basement within the initial oceanic domain alongside the conjugate Flemish Cap and GS margins shows roughness values typical of slow-spreading ridges. We also show that the roughness and morphology of the top basement alongside the conjugate Australian and Antarctic margins indicate large tectonic extension and intermediate magma supply at either slow or ultraslow-spreading rates.

2 DATA AND METHOD

The stochastic modelling procedure (Goff & Jordan 1988, 1989) offers a robust way to analyse the statistical properties of abyssal hill morphology. This method was applied on grids of

bathymetric data that were collected using multibeam echo sounders on the flanks of the MAR (Goff 1991; Goff *et al.* 1995; Neumann & Forsyth 1995) and the SWIR (Sauter *et al.* 2011; Sloan *et al.* 2012). Close to the ridge axis and far from continents, where sediments are lacking, such bathymetric grids allow a 2-D analysis of the top of the oceanic crust. On sedimented rifted margins or spreading ridges, MCS profiles are needed to investigate the top basement relief, but are spaced too far apart and give only access to 1-D analysis of the top basement. Nevertheless, calculation of the roughness of the top basement is derived the same way from 1-D or 2-D data. It is defined as the root-mean-square (RMS) height, which is the average variation of depths with respect to the regional depth trend. RMS height is therefore calculated after removing the regional trend from the data. We used a second order empirical trend of the basement instead of a theoretical subsidence curve to avoid dependence upon on a crustal age model (Ehlers & Jokat 2009).

When available we use MCS data published as depth sections (Hopper *et al.* 2004; Bullock & Minshull 2005; Shillington *et al.* 2006; Gerlings *et al.* 2012; Dean *et al.* 2015; Tugend *et al.* 2015). However, MCS data are commonly shown as two-way traveltime (TWTT) sections (e.g. Afilhado *et al.* 2008; Welford *et al.* 2010b, Pickup *et al.* 1996). The seafloor and top basement reflections were thus picked to obtain the sediment thickness in second TWTT which was then depth converted and added to the seafloor bathymetry to obtain the top basement relief in meters. Sediment velocity information was provided by a compilation of wide angle and refraction seismic sections within each area of interest. Along the Iberia margin we use the TWTT-velocity relationships of (Cunha 2008) to convert MCS data in the Iberia Abyssal Plain (IAP; Pickup *et al.* 1996) and in the Tagus Abyssal Plain (TAP; Afilhado *et al.* 2008). On the Newfoundland margin, we built up on the work of (Shillington *et al.* 2006; van Avendonk *et al.* 2006) and (Hopper *et al.* 2004) to determine the TWTT-velocity functions for the SCREECH 2 and SCREECH 1 areas that were then used to derive the depth of the top basement for the MCS data falling within these areas (Welford *et al.* 2010b). No refraction profile has been collected on the conjugate Australian-Antarctic margins. Therefore we used compilations of velocity profiles from sonobuoys (Ball 2005; Gillard 2014) to derive TWTT-velocity functions and convert MCS data interpreted by Gillard *et al.* (2015, 2016a,b).

3 SEAFLOOR ROUGHNESS AT ULTRASLOW-SPREADING RIDGES

We review hereafter the top basement roughness estimates at the SWIR, Gakkel, Knipovich and Sheba ridges, the MCSC, the SPR and the MAR (Table 1). We focus first on the SWIR as there, roughness values are well documented on various tectonic settings (Sauter *et al.* 2011; Sloan *et al.* 2012). The presence of exhumed mantle-derived rocks on >100 km long stretches of the ridge axis is one of the striking contrasts between most of the ultraslow-spreading ridges and faster spreading ridges (Dick *et al.* 2003; Sauter *et al.* 2004, 2013; Cannat *et al.* 2006). However, exhumed mantle is not ubiquitous at ultraslow-spreading ridges and thick magmatic oceanic crust is also found there (Niu *et al.* 2015). Although some fossil oceanic ridges have undergone slow to ultraslow rates while spreading was failing (e.g. in the Labrador or Somali basin) we disregarded them as a post spreading tectonic phase may have affected the top basement (Delescluse *et al.* 2015; Sauter *et al.* 2016).

3.1 The Southwest Indian ridge (SWIR)

The SWIR full spreading rate has been ultraslow since a dramatic decrease ∼24 myr ago, from a slow rate of 30 to 15 mm yr^{-1} (Patriat *et al.* 2008). The RMS abyssal hill height mean value (298 m; Table 1), determined within polygonal areas on the flanks of the eastern part of the ultraslow-spreading SWIR, is ∼80 m greater than for slow-spreading seafloor. However, seafloor roughness also increases eastward along the SWIR axis (Sauter *et al.* 2011). The roughness mean value (372 m) is much larger between 61 and 67°E, in the easternmost deep part of the ridge, than between 54 and 61°E (242 m; Table 1). Fig. 2 displays some bathymetric profiles to illustrate this eastward increasing roughness of the seafloor. The Mantle Bouguer Anomaly (MBA; a crustal thickness and/or mantle temperature proxy deduced from gravity data) also changes eastward, suggesting thinner crust and/or cooler mantle temperatures in the easternmost part of the SWIR (Sauter *et al.* 2011). There, large seafloor domains of exhumed mantle derived rocks have been called 'smooth seafloor' because they occur in the form of broad ridges with a smooth, rounded topography with no resolvable volcanic cones or typical abyssal hills on bathymetric data (Cannat *et al.* 2006). The mean value of RMS height for these exhumed mantle domains (304 m) is ∼70 m smaller than for the volcanic seafloor (372 m; Sloan *et al.* 2012; Table 1 and Fig. 2).

Seafloor roughness could not be estimated in the shallowest part of the SWIR (35–52°E) where the magmatic crust is the thickest (Zhao *et al.* 2013; Niu *et al.* 2015). There, a sudden increase of the magma supply ∼10 Ma ago is thought to have resulted in a shallow volcanic plateau at the ridge axis (Sauter *et al.* 2009). This plateau is too narrow to estimate valid roughness values. However, we note that large topographic features (up to 60 km long and ∼900 m-high) are observed on top of this volcanic plateau as well as close to the Marion hot spot (Mendel *et al.* 2003) suggesting still thick lithosphere in the shallowest parts of the SWIR.

3.2 The arctic ridges

High roughness values (>500 m) were obtained by Weigelt & Jokat (2001) and Ehlers & Jokat (2009) along >100 km long seismic reflection profiles in the Arctic Ocean. We retain nine seismic profiles in the Amundsen, Nansen and Boreas basins on the flanks of the ultraslow-spreading Gakkel and Knipovich ridges (9–15 mm yr^{-1} spreading rates) and disregard one profile in the Molloy basin as it is located too close to the Spitsbergen Fracture Zone. The roughness values were estimated from profiles of seismically determined top basement by (Weigelt & Jokat 2001; Ehlers & Jokat 2009). They may not be straightforwardly compared to the statistical analysis of bathymetric grids at the SWIR. However, the mean roughness value on the ultraslow-spreading Arctic ridges is significantly larger (517 m; Table 1) than those estimated on the SWIR (Fig. 2). No correlation has been found between these values and the magmatic and amagmatic segmentation of the Arctic ridges or the highly variable thickness of the crust (2–6 km; Ehlers & Jokat 2009).

3.3 The Mid-Cayman Spreading Center (MCSC)

The deep-seated MCSC is located midway along a depression, called Cayman trough, that extends from the Belize margin to the northern edge of Jamaica. Seafloor magnetic anomalies within the Cayman trough record a ∼17 mm yr^{-1} ultraslow-spreading rate for

Table 1. Estimations of the top basement roughness on ultraslow-spreading mid-oceanic ridges.

	Full Rate (mm yr^{-1})	RMS height (m)	Size and type of data set	Number of samples	References
Southwest Indian Ridge (SWIR)	15		∼100 km long bathymetric grids		(Sauter *et al.* 2011; Sloan *et al.* 2012)
54–67°E (volcanic domains)	15	298 ± 23	id.	27	id.
54–61°E (volcanic domains)	15	242 ± 36	id.	12	id.
61–67°E (volcanic domains)	15	372 ± 23	id.	9	id.
61–67°E (exhumed mantle domains)	15	304 ± 20	id.	6	id.
Arctic ridges	9–15	517 ± 50	>100 km long MCS profiles	9	(Weigelt & Jokat 2001; Ehlers & Jokat 2009)
Mid-Cayman Spreading Center (MCSC)	17	371 ± 79[a]	>120 km long bathymetric profiles	13	GeoMapApp cruises
Western flank	17	432 ± 72[a]	id.	6	id.
Eastern flank	17	319 ± 34[a]	id.	7	id.
Sheba ridge 52–55°E	20	164 ± 59[a]	>140 km long MCS profiles	3	(d'Acremont *et al.* 2010)
Western basin	20	103[a]	150 km long MCS profile	1	id.
Eastern basin	20	195 ± 50[a]	>140 km long MCS profiles	2	id.
Mid Atlantic Ridge (MAR)	18		>100 km long MCS profiles	3	
Western North America basin	18	257[a]	>130 km long MCS profile	1	(Lizarralde *et al.* 2004)
Western North America Basin	18	160	>100 km long MCS profile	1	(Min 1999 1999)
Eastern (Canary) basin	18	350	id.	1	id.
South Pandora Ridge (SPR)	18	158 ± 16[a]	>80 km long bathymetric grids	4	(Lagabrielle *et al.* 1996)

[a]Determined in this paper. Values with standard deviations are mean values.

the last 20 myr (Leroy *et al.* 2000). Series of horsts and grabens are well marked about 150 km on either side of the N–S oriented spreading centre but, further away, the seafloor topography becomes smoother as the sedimentary cover thickens towards the Belize margin to the west and offshore Cuba Island to the east (Leroy *et al.* 2000). We therefore use 13 ∼125 km long-bathymetric profiles from the WI93300 and Ka93200 cruises (from USNS Wilkes and Kane in 1973 and 1972 respectively) on each flank of the MCSC excluding a 60 km wide central part across the ridge axis. The bathymetry of the off-axis Cayman trough is highly asymmetric (Hayman *et al.* 2011). The estimated roughness to the west of the MCSC is larger (432 m mean value) than to the east (319 m mean value; Table 1). The crustal thickness is thought to be also asymmetric, with thinner upper crust to the east than to the west (Leroy *et al.* 1996; Hayman *et al.* 2011). However, we choose to disregard the crustal thickness estimations on the MCSC as they are poorly constrained and debated (ten Brink *et al.* 2002).

3.4 The Sheba ridge

The 20–22 mm yr^{-1} spreading rate of the Sheba ridge is equal to the threshold (Fournier *et al.* 2001; Leroy *et al.* 2004) below which the ultraslow-spreading class of oceanic ridges is usually defined (Reid & Jackson 1981). We use the top basement relief determined in two seismic profiles from the Arabian margin to the Somalian margin between the Alula-Fartak Fracture Zone and the Socotra-Hadbeen Fracture Zone (d'Acremont *et al.* 2010). We avoid the axial valley relief and exclude thus a central 100 km wide part to estimate the roughness of the oceanic crust. We also disregard the anomalously shallow area on the southern flank of the Sheba ridge where recent off-axis volcanism has been shown by (Leroy *et al.* 2010a). The estimated mean roughness value is larger in the eastern basin (195 m mean value; Table 1) than in the western one (103 m), while the crust is thinner in the eastern than in the western basin (4 and 6 km average crustal thickness, respectively; Leroy *et al.* 2010b, d'Acremont *et al.* 2010; Watremez *et al.* 2011).

3.5 The South Pandora ridge (SPR)

The North Fiji Basin is a back-arc basin opening with a complex geometry of spreading centres trending both ∼NS and ∼EW (Garel *et al.* 2003). We used a set of multibeam bathymetric data collected along the 500 km long SPR, which is opening with an ultraslow-spreading rate (16 mm yr^{-1}; Lagabrielle *et al.* 1996). We obtained a low RMS roughness mean value (158 m; Table 1). It is worth pointing out that the SPR strongly differs from other ultraslow-spreading ridges. Mantle rocks have never been recovered along any segment of the ridges of the North Fiji Basin (Garel *et al.* 2003)

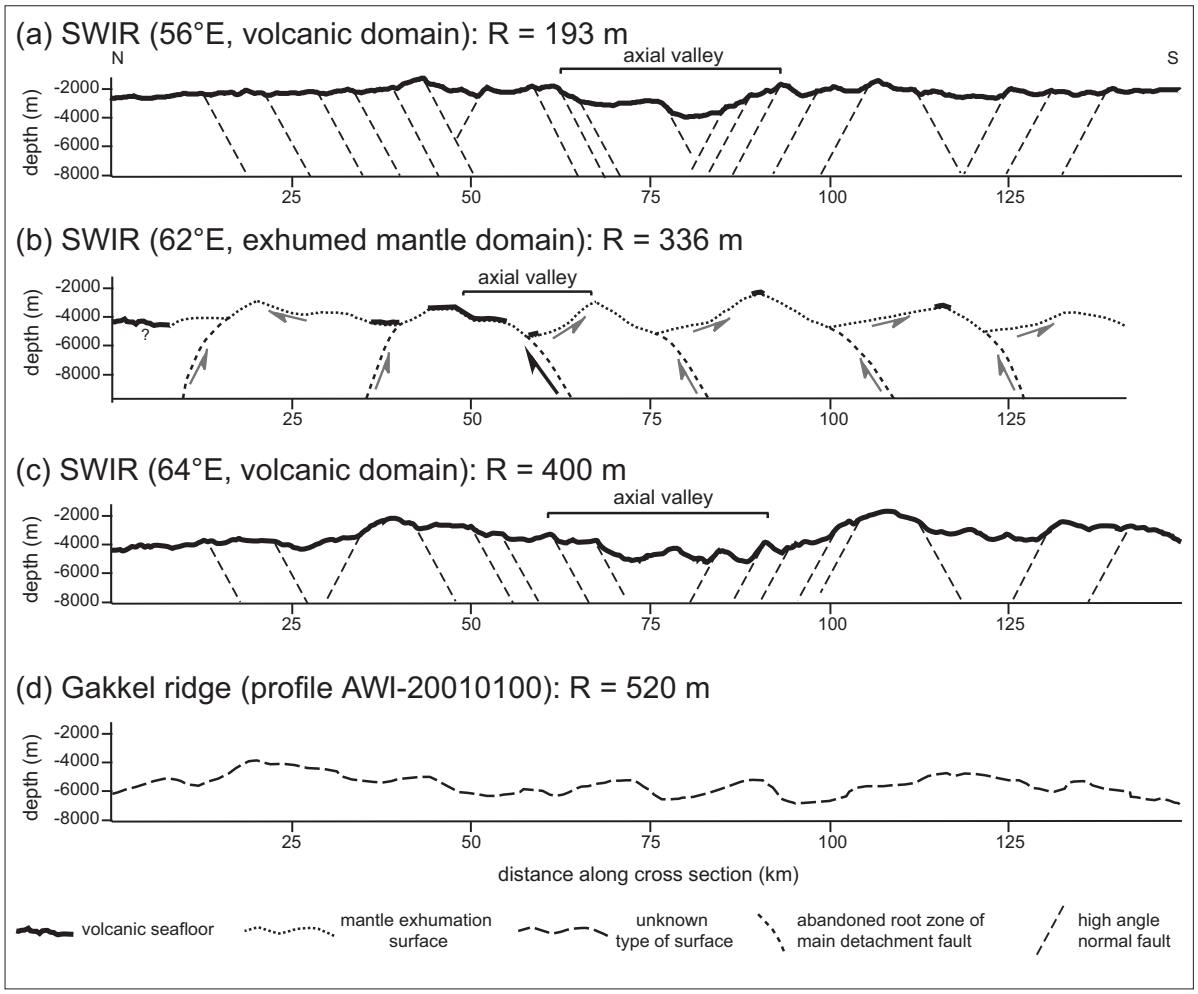

Figure 2. Across axis profiles at the Southwest Indian Ridge and the Gakkel ridge illustrating the range of roughness values (R) found at ultraslow-spreading centres. (a) Bathymetric profile crossing the SWIR ridge axis (at 56°E) showing a roughness value <200 m (calculated outside the axial valley; see Sauter *et al.* 2011) and typical abyssal hills usually observed at slow-spreading centres; (b) bathymetric profile (at 62°E) in the easternmost magma-poor section of the ridge within a domain of exhumed mantle derived rocks (smooth seafloor); (c) bathymetric profile crossing the SWIR axis (at 64°E) within a volcanic part of the easternmost magma-poor section of the ridge; (d) top basement picked in the seismic reflection profile AWI-20 010 100 on the eastern flank of the Gakkel ridge. Fault locations are inferred from the bathymetric grids. Their depth and dip are unconstraint. Vertical exaggeration is 2×. Profiles across the SWIR are from Sauter *et al.* (2009) and Sauter *et al.* (2013). The roughness values estimated along the SWIR bathymetric profiles are slightly different from the roughness values given in Table 1 which are mean values calculated on several polygonal areas. The roughness estimation and the profile on the flank of the Gakkel Ridge are from (Ehlers & Jokat 2009).

contrasting with the frequent recovery of serpentinized peridotites at segment ends along the ultraslow and slow oceanic ridges (e.g. Cannat 1993). Moreover, the magma production is high, consistent with the general shallow depth of the entire back arc basin and the analysis of gravity anomalies indicating crustal thickness as large as 8 km along the SPR (Garel *et al.* 2003).

3.6 The Mid Atlantic ridge (MAR)

The spreading rate in the North Atlantic decreased by a factor of about two between M-21 (148 Ma) and M-11 (135 Ma; Sundvik *et al.* 1984). A rough acoustic basement is associated with this period of ultraslow-spreading (~18 mm yr^{-1}) in the Central Atlantic west of Bermuda and in the conjugated Canary Basin (Sundvik *et al.* 1984; Ranero & Banda 1997). Min (1999) estimated that the RMS roughness mean values only increased from 130 to 160 m in the Western (Central Atlantic) Basin while it reached ~350 m in the eastern (Canary) Basin. Using the MCS data of Lizarralde *et al.* (2004) collected in the Western Basin we obtained a higher roughness value of 257 m for the ultraslow-spreading basement (Table 1). Refraction data coincident with the MCS in the western North Atlantic basin show that the crustal thickness decreased from 6.7 to 5.5 km when spreading became ultraslow (Lizarralde *et al.* 2004).

Finally, as a conclusion of this section, we note that the roughness estimations obtained at these ultraslow-spreading ridges cover a wide range of values, from ~100 m on the Sheba Ridge to ~580 m in the Arctic basin (Weigelt & Jokat 2001).

4 TOP BASEMENT ROUGHNESS ALONGSIDE MAGMA-POOR MARGINS

Estimating the roughness of initial oceanic crust alongside rifted margins requires to define the location of the Continent Ocean Boundary (COB). Typically, 'normal' oceanic crust is characterized in MCS sections by a: (1) smooth top basement at a kilometric scale, commonly observed at 8 s TWTT, (2) highly reflective upper

Table 2. Estimations of the top basement roughness within the initial oceanic domain alongside magma-poor rifted margins. OC, Oceanic crust; EM, exhumed mantle; POC, proto-oceanic crust (see definition in main text).

	Inferred crust type	RMS height (m)	Profile length (km)	Number of profiles	References
Tagus Abyssal Plain (TAP)				1	
Shallow subdomain on IAM5 line	OC	456[a]	60	1	(Afilhado *et al.* 2008)
Deep subdomain on IAM5 line	OC	414[a]	105	1	id.
Both domains on IAM5 line	OC	520[a]	165	1	id.
Iberia Abyssal Plain (IAP)				3	
West of R4 on IAM9 line	OC	429[a]	80	1	(Pickup *et al.* 1996)
East of R4 on IAM9 line	EM	368[a]	115	1	id.
West of R3 on Lusigal12 line	OC	566[a]	120	1	(Beslier 1996)
West of R3 on SO-22 line	OC	534[a]	160	1	(Pickup *et al.* 1996)
Mean Value for OC	OC	510 ± 72[a]		3	id.
Galicia Margin (GM)					
West of Peridotite Ridge on line WE1	OC	583[a]	85	1	(Dean *et al.* 2015)
Northern Newfoundland Basin (NNFB)				5	
East of M0 on SCREECH 2	OC	449[a]	75	1	(Shillington *et al.* 2006)
West of M0 on SCREECH 2	EM	410[a]	120	1	id.
West of M3 on SCREECH 2	EM	268[a]	75	1	
East of M0 on SCREECH 107/201	OC	355[a]	80	1	id.
East of M0 on SCREECH 302/109	OC	374[a]	84	1	id.
East of M0 on SCREECH E56	OC	320[a]	75	1	(Welford *et al.* 2010b)
West of M0, on SCREECH E56	EM	378[a]	96	1	
East of M0 on SCREECH E54	OC	320[a]	144	1	id.
Mean value for OC	OC	364 ± 53[a]		5	id.
Mean value for EM	EM	394 ± 23[a]		3	id.
Southern Margin of Flemish Cap (SMFC)				1	
On line E36	OC	380[a]	93	1	(Welford *et al.* 2010b)
Northern Margin of Flemish Cap (NMFC)				2	
On line F87–4	OC	215[a]	85	1	(Welford *et al.* 2010a)
On line F87–3	OC	322[a]	87	1	id.
Goban Spur Margin (GS)				1	
On WAM line	OC	216	50	1	(Bullock & Minshull 2005)
On WAM	EM	128	67	1	id.
Bay of Biscay (BB)				3	
On Norgasis 11–12	OC	315[a]	65	1	(Thinon *et al.* 2003)
On Norgasis 14	OC	275[a]	64	1	id.
On IAM12	OC	328[a]	95	1	(Tugend *et al.* 2014)
Great Australian Bight (GAB)				8	
On GA199–10	POC	231[a]	56	1	(Gillard *et al.* 2015)
On GA199–10	OC	258[a]	102	1	id.
On GA199–07	POC	251[a]	61	1	id.
On GA199–06	OC	243[a]	96	1	id.
On GA199–06	POC	362[a]	61	1	id.
On GA199–05	POC	262[a]	82	1	id.
On GA199–04	POC	216[a]	82	1	id.
On GA199–03	POC	374[a]	99	1	id.
On GA199–02	POC	356[a]	95	1	id.
On GA199–01	POC	313[a]	106	1	id.
On GA199–01	OC	296[a]	117	1	id.
Mean value for POC	POC	296 ± 63[a]		8	id.
Mean value for OC	OC	266 ± 27[a]		3	id.
Wilkes Land Basin (WLB)				6	
On GA228–27	POC	333[a]	143	1	id.
On GA228–26	POC	336[a]	163	1	id.
On GA228–26	OC	208[a]	57	1	id.
On GA228–25	POC	270[a]	60	1	id.
On GA228–24	POC	298[a]	129	1	id.
On GA228–23	POC	256[a]	154	1	id.
On GA228–22	POC	313[a]	83	1	id.
On GA228–22	OC	269[a]	50	1	id.
Mean value for POC	POC	301 ± 33[a]		6	id.
Mean value for OC	OC	239 ± 43[a]		2	id.

[a]Determined in this paper.

crust and an acoustically relatively transparent lower-crust, (3) ∼2 s TWTT thickness, (4) well-marked reflector at the base of the crust interpreted as the Moho, commonly observed at 10 s TWTT and (5) passive sediment infill (e.g. Klimke *et al.* 2016). However, seismic reflection profiles beyond rifted margins often do not sample such unambiguous oceanic crust. A well-marked reflector that could be interpreted as the Moho is rarely observed, while the seismic texture within the basement is often confusing. Therefore, initial oceanic crust is usually inferred from a conjunction of arguments from seismic (refraction and/or reflection) as well as potential field data, none of these being conclusive on its own. This is the case at the Iberia–Newfoundland, GS–Flemish Cap, BB, and Australo–Antarctic margin systems that we analyse hereafter (Table 2). Although we use the location of the initial oceanic domains proposed in the literature, we were careful to verify some basic characteristics. As the COB can be associated with an important top basement topography (Unternehr *et al.* 2010), thought to result from the transition from a deep and denser exhumed mantle domain to a shallower less dense oceanic domain (Peron-Pinvidic *et al.* 2013), we checked that the location of such topographic features agrees with the inferred location of the COB. Moreover, domains with volcanic overprint and/or a deformed sediment cover were not assumed to be oceanic in nature as no deformation related to spreading is expected on the flanks of mid-oceanic ridges outside a narrow deformation zone close to the axis (Cannat *et al.* 2009).

4.1 The Iberia margin

Because the J magnetic anomaly is thought to be located at the boundary between exhumed mantle and initial oceanic crust in the IAP, it has been proposed to mark the limit of the oceanic domain in the whole Iberia–Newfoundland system (Bronner *et al.* 2011; Stanton *et al.* 2016). However, (Nirrengarten *et al.* 2017) recently demonstrated that the J anomaly is the result of polygenic and multiple magmatic events occurring during and after the formation of initial oceanic crust. We therefore built on the COB proposed by Nirrengarten *et al.* (2017) that uses a combination of geophysical and geological arguments.

4.1.1 The Tagus Abyssal Plain (TAP)

In the TAP a two-layer igneous oceanic crust was recognized at the IAM5 MCS line and the wide-angle data by (Afilhado *et al.* 2008). A sharp step of the top basement marks the limit between a westernmost shallow subdomain and a deeper easternmost subdomain (see Plate 1 of Afilhado *et al.* 2008). MCS reflections were inferred between 10 and 11 s TWT, consistent with the Moho depth obtained from velocity models (Afilhado *et al.* 2008). The inferred crustal thickness of the initial oceanic crust increased westward from 5 km on average in the deep subdomain to 7 km on average in the shallow one (Afilhado *et al.* 2008). Therefore, (Nirrengarten *et al.* 2017) took the basement step between the two subdomains as indicating the transition to an unambiguous magmatic oceanic crust. Excluding the western termination of IAM5 line at the volcanic Tore Madeira rise, we estimated the roughness values in the shallow and the deep subdomains to 456 and 414 m, respectively (Table 2). Analysing the shallow and deep subdomains together leads logically to a higher roughness value of 520 m.

4.1.2 The Iberia Abyssal Plain (IAP)

Three MCS lines, IAM9, SO-22 (Pickup *et al.* 1996) and Lusigal12 (Beslier *et al.* 1996), reach the oceanic domain in the IAP. Constrains are given by refraction data and several drill holes drilled during ODP Legs 149 and 173 (Dean *et al.* 2000; Whitmarsh *et al.* 2001; Minshull *et al.* 2014). The refraction data show that the inferred initial oceanic crust is 6–7 km thick (Minshull *et al.* 2014). The transition between the initial oceanic crust to the west and the exhumed mantle domain to the east is marked by a series of peridotite ridges on MCS lines (Pickup *et al.* 1996). The peridotite ridges called R3 and R4 by (Pickup *et al.* 1996) mark the beginning of the westward shallowing of the top basement on the MCS lines. The roughness mean value for the initial oceanic crust to the west of these ridges is estimated at 510 m (Table 2). Taking anomaly J instead of the peridotite ridge R3 as the COB on the SO-22 profile results in a similar roughness value for initial oceanic crust (520 m versus 534 m using R3) although the sub-section is 50 km shorter. Because the exhumed mantle domains on the Lusigal12 and SO-22 lines were too short, we estimate the roughness over the exhumed mantle domain (at 368 m) only using the IAM9 profile.

4.1.3 The deep Galicia margin

As in the IAP the transition between the initial oceanic crust and the exhumed mantle domain is marked by a series of peridotite ridges. On MCS line WE1 (Dean *et al.* 2015) suggested a gradual transition to seafloor spreading westward of the 'Peridotite Ridge' (Fig. 3) where the top basement begins to shallow. There, recently published refraction data suggest a very thin oceanic crust thickening seaward (∼0.5–1.5 km; Davy *et al.* 2016). Oceanic layer 3 is absent and the crust is thought to overlie serpentinized mantle material (Davy *et al.* 2016). The roughness value estimated to the west of the Peridotite Ridge is 583 m (Fig. 3).

4.2 The Newfoundland margin

We focus here on the Northern Newfoundland Basin (NNFB) and on the Southern margin of Flemish Cap (SMFC). Because oceanic crust is overprinted by post breakup magmatism in the Newfoundland Seamounts area, we disregard the Southern Newfoundland Basin.

4.2.1 The Northern Newfoundland Basin (NNFB)

Refraction data in the NNFB show that the landward limit of a 3 km thick oceanic crust falls close to the eastern end of the J anomaly (interpreted as M0; van Avendonk *et al.* 2006; Welford *et al.* 2010b). Layer 3 oceanic crust is interpreted to be missing with layer 2 directly overlying serpentinized mantle (van Avendonk *et al.* 2006). Normal oceanic crust of 6 km thickness is thought to be found at the seaward ends of the MCS lines of the SCREECH project, but a continuous Moho reflection is not observed. As along the Iberia margin, the transition between the oceanic crust and the exhumed mantle domain is marked by a series of peridotite ridges on the MCS lines. There, at ODP Site 1277, drilling into basement revealed gabbro and basalt fragments as well as serpentinized peridotites of subcontinental origin (Tucholke & Sibuet 2007). We use three MCS lines of the SCREECH project (SCREECH 2, 107/201 and 302/109; Shillington *et al.* 2006) and E56 and E54 lines of the Erable project in the NNFB (Welford *et al.* 2010b; Fig. 3). The mean roughness value for the oceanic crust east of M0 is estimated at 364 m while the mean roughness value for the exhumed mantle domain west of M0 is estimated at 394 m (Table 2). Moving the COB to the western end of the J anomaly (interpreted as M3) as suggested by (Shillington *et al.* 2006) on SCREECH 2 profile results in a similar estimation for the roughness of the oceanic crust

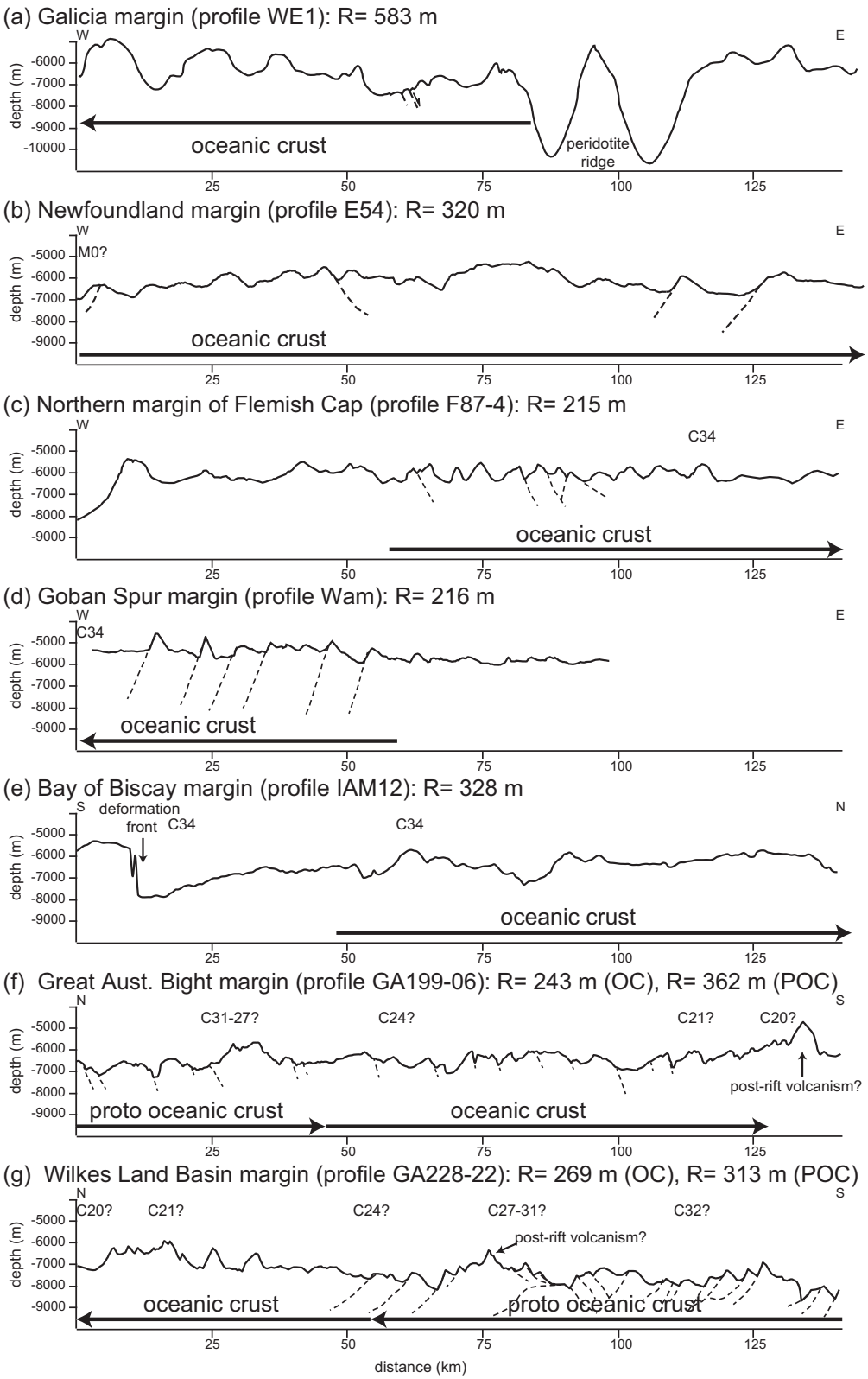

Figure 3. Top basement relief in initial oceanic crust alongside magma-poor rifted margins. Roughness (*R*) is estimated for oceanic crust (OC) and proto-oceanic crust (POC) along MCS profiles of the (a) Galicia margin (profile WE1 from Dean *et al.* 2015); (b) Newfoundland margin (profile Erable54 from Welford *et al.* 2010b); (c) Northern margin of Flemish Cap (profile F87–3 from Welford *et al.* 2010a); (d) Goban Spur margin (profile WAM from Bullock & Minshull 2005); (e) Cantabrian margin in the Bay of Biscay (profile IAM12 from Tugend *et al.* (2014); (f) Great Australian Bight margin (profile GA199–06 from Gillard *et al.* 2015); (g) Wilkes Land margin (profile GA228–22 from Gillard *et al.* 2015). Vertical exaggeration is 2×.

than using the eastern end of the J anomaly (458 m and 449 m, respectively), although the sub-section is 50 km shorter. Excluding the outer high drilled by the IODP Site 1277 that has been formed after the exhumation stage (Bronner *et al.* 2011) leads to much lower roughness values for the exhumed mantle domain (268 m on SCREECH 2).

4.2.2 The Southern Margin of Flemish Cap (SMFC)

At the SMFC, (Hopper *et al.* 2004) interpreted the last ~80 km at the seaward end of the MCS line SCREECH 1 as oceanic crust whereas a recent reinterpretation suggested a much narrower oceanic domain (<15 km; Gillard *et al.* 2016b). Both interpretations are compatible with the seismic refraction data along this line (Funck *et al.* 2003). Instead, we use here the Erable E36 MCS line that enters the initial oceanic domain over >90 km to the east of the J anomaly according to (Welford *et al.* 2010b). Roughness is estimated at 380 m over this domain (Table 2). Distinguishing anomalously thin oceanic crust (with 3 km thickness) and normal oceanic crust (with 6 km thickness (Funck *et al.* 2003; Hopper *et al.* 2004)) along E36 line brings slightly lower roughness values of 351 and 344 m, respectively.

4.3 The Northern margin of Flemish Cap (NMFC) and the Goban Spur (GS) conjugate margin

The Flame Lines F87–3 and F87–4 cross magnetic anomaly 34 at the NMFC and extend another ~50 km seaward well into oceanic crust (Welford *et al.* 2010a). Refraction data along profile F87–3 show a two-layer oceanic crust that is somewhat thinner (4.5–6.5 km) than typical oceanic crust (Gerlings *et al.* 2011). Roughness values for the oceanic crust are estimated at 322 and 215 m along F87–3 and F87–4 profiles, respectively (Table 2). The Western Approaches Margin (WAM) line on the GS margin is thought to be conjugate of the F87–3 line (Welford *et al.* 2010a; Gerlings *et al.* 2012). The Flemish Cap and GS conjugate margins form an asymmetrical pair: the exhumed mantle domain is ~100 km wide off GS (Bullock & Minshull 2005) while it is narrower (~25 km) on the NMFC (Welford *et al.* 2010a). The exhumed mantle domain off GS has a low relief basement (with a very low roughness of 128 m, Table 2) that has been interpreted as a detachment surface (Whitmarsh *et al.* 2001). In the region of initial oceanic crust off GS, the basement is shallower and has a more subdued relief than that off Flemish Cap along F87–3 line. There, (Bullock & Minshull 2005) estimated the roughness value for a ~6 km thick initial oceanic crust off GS at 216 m (Fig. 3). A similar low roughness value (215 m) and a normal thickness oceanic crust (inferred from gravity data; Welford *et al.* 2010a) are found at the seaward end of the F87–4 profile (Fig. 3).

4.4 The Bay of Biscay (BB)

The BB is characterized offshore by an oceanic basin where spreading began at Aptian-Albian time and stopped at Santonian time (e.g. Tugend *et al.* 2014, and references therein). We use Norgasis 11–12 and 14 MCS lines across the Armorican Margin (Thinon *et al.* 2003; Tugend *et al.* 2014, 2015) and the IAM12 MCS line across the North Iberian Margin (Alvarez-Marron *et al.* 1997; Tugend *et al.* 2014) excluding the failed ridge axis and areas too close to the compressional accretionary prism (Fernández-Viejo *et al.* 2012). Roughness values were estimated at 275 and 315 m for the Norgasis lines and at 328 m for the IAM12 line (Fig. 3). Refraction data along Norgasis 14 line show a 3–5 km thick ocean crust at the southern end of the line while a normal ~6 km thick oceanic crust is found at the northern end of IAM12 line (Fernández-Viejo *et al.* 1998; Thinon *et al.* 2003).

4.5 The Australia-Antarctic margin system

There is an ongoing debate on the location and age of the first undisputable oceanic crust within each sector of the Australian-Antarctic margin system (Tikku & Cande 1999; Tikku & Direen 2008). We focus here on the Great Australian Bight (GAB)—Wilkes Land Basin (WLB) system using Australian MCS lines from the AGSO surveys GA199 and GA228 (e.g. Sayers *et al.* 2001). In both the GAB and the WLB, Gillard *et al.* (2015) used these MCS lines to distinguish a 'proto-oceanic' domain from a 'steady-state' oceanic domain. This so-called proto-oceanic domain is interpreted as composed of hybrid crust (exhumed mantle and magmatic rocks) and formed as a non-steady state, not localized seafloor spreading. The steady-state oceanic domain is formed from stable oceanic accretion. The proto-oceanic crust is characterized by a deformed base of the sedimentary coverture, the presence of volcanic additions sealing faults, and the rise of the top basement arguing for an increase of magmatism. The oceanic Moho is absent in the proto-oceanic crust but is observed locally at ~10 s (TWT) in the steady state oceanic crust (Gillard *et al.* 2015). However, by contrast to the Iberia–Newfoundland system, the nature of the basement is ill defined at the GAB/WLB system as neither refraction data nor samples can confirm the inferred basement type. For the GAB, the mean roughness values of the top basement on eight MCS lines in the proto-oceanic and steady-state oceanic domains are estimated at 296 and 266 m, respectively (Table 2, Fig. 3). In the basin off the Wilkes Land we used six MCS lines to estimate the mean roughness values at 301 and 239 m for the proto-oceanic and steady-state oceanic domains, respectively (Table 2, Fig. 3). Within the initial oceanic crust alongside both margins, we exclude large conic-shaped edifices that we interpreted as resulting from post-rift volcanic activity (Fig. 3).

As a conclusion of this section, we note that, as for ultraslow-spreading ridges, the roughness estimations obtained over initial oceanic domain alongside magma-poor rifted margins cover a wide range of values, from ~210 m in the Wilkes Land Basin to ~580 m off the Galicia margin.

5 COMPARISON OF OCEANIC BASEMENT ROUGHNESS AT MID-OCEAN RIDGES AND OVER INITIAL OCEANIC DOMAIN ALONGSIDE MAGMA-POOR RIFTED MARGINS

5.1 Clues from mid-oceanic ridges

5.1.1 Top basement roughness versus spreading rate

It is well known that the elastic lithosphere along slow-spreading ridges is relatively thicker than at faster spreading ridges (Chen & Morgan 1990) and is thus able to sustain greater relief through faulting and flexure (Shaw & Lin 1996). The 750 °C isotherm obtained by thermal modelling for fast to slow-spreading ridges correlates well with the spreading-rate dependence inferred from

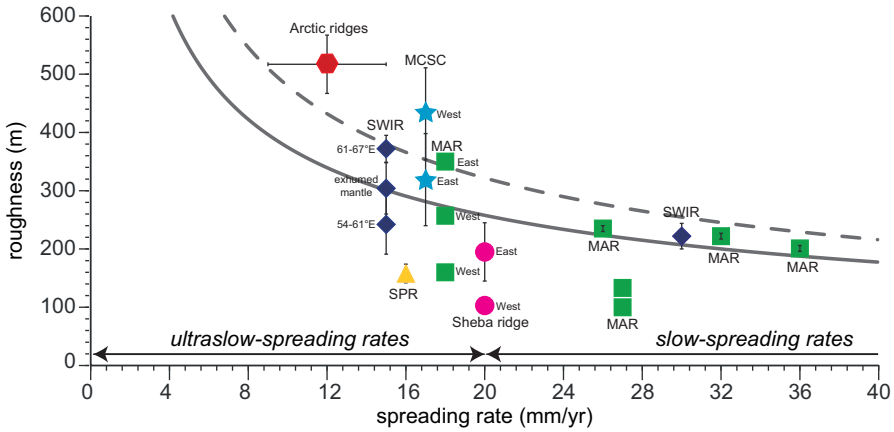

Figure 4. Roughness versus spreading rate for ultraslow and slow-spreading ridges. Data for ultraslow-spreading ridges are given in Table 1. Those for the slow-spreading Mid Atlantic Ridge are from (Goff 1991; Goff *et al.* 1995; Neumann & Forsyth 1995; Min 1999). The roughness value for the slow-spreading SWIR (before 24 Ma) is from Sauter *et al.* (2011). The continuous grey line is the power-law curve fit of (Malinverno 1991) and the dashed grey line is the curve fit of Ehlers & Jokat (2009).

teleseismic axial earthquake depths (from 2 to 10 km depth; Phipps Morgan & Chen 1993). A recent study of the seismicity along ridge sections of the SWIR and Arctic ridges revealed that earthquakes reach maximum depths of 15 km below volcanic segments and as much as 35 km below the sea floor in exhumed mantle domains (Schlindwein & Schmid 2016). This shows that the lithosphere can be much thicker at ultraslow-spreading ridges than at slow ones.

Early attempts to analyse the relationship between the roughness of oceanic seafloor and spreading rate suffered from the lack of data for ultraslow-spreading crust (Small 1994; Goff *et al.* 1997). The new roughness values of seafloor collected in this paper supplement the global data for the ultraslow end of the spectrum. Fig. 4 shows these values compared to the power-law curve fit of (Malinverno 1991) obtained for slow to fast spreading rates. (Ehlers & Jokat 2009) noted that the roughness values obtained for the Arctic ridges were systematically above this reference curve and thus proposed an updated curve fit for slow and ultraslow-spreading crust. The mean roughness values obtained at the ultraslow-spreading SWIR, MCSC, MAR, SPR, Arctic and Sheba ridges range from 100 to >500 m and fall well above or below these two reference curves. The roughness of the flanks of the SPR and the Sheba ridge are even lower than 200–240 m, which is typical of slow-spreading ridges (e.g. at the MAR; Goff *et al.* 1997). This scattering supports that, although the oceanic basement roughness generally increases as the spreading rate decreases from slow to ultraslow, this variation is not solely related to spreading rate (e.g. Goff *et al.* 1997).

5.1.2 Top basement roughness versus magma supply

A weak correlation between spreading rate and bathymetric roughness was also observed at slow-spreading centres, while roughness is relatively constant for intermediate to fast spreading ridges (Small 1994). This weak correlation has been attributed to the along-axis variable thickness of magmatic crust resulting in a more heterogeneous bulk rheology of the lithosphere at slow-spreading ridges than at faster ridges (Small 1994). Along the eastern SWIR, the west-to-east increase of the roughness toward the magma-poor easternmost section (Fig. 4) correlates well with increasing MBA values indicating progressively thinner magmatic crust and/or cooler mantle temperatures (Sauter *et al.* 2011). Either case should produce progressive strengthening of the lithospheric mantle: reduction of the thickness of the magmatic crust relative to the rigid upper mantle will strengthen the lithosphere while the decrease in mantle temperature should produce increasing lithosphere thickness since elastic strength of the lithosphere is dependent upon thermal structure. On the Sheba ridge, roughness is also larger in the ridge section where the crust is thinner (d'Acremont *et al.* 2010). However, no such correlation have been found for the Arctic ridges (Ehlers & Jokat 2009) and no well constrained thickness estimations are available for the MSCS.

Despite few estimations of crustal thickness along ultraslow ridges, Fig. 5 shows a weak tendency for increasing roughness when magmatic crustal thickness decreases. The wide range of crustal thickness at ultraslow-spreading ridges shows that another process than enhanced cooling of the mantle when spreading rate decrease is required. A thickening of the thermal boundary layer at those ridges does reduce the height of the melting regime and thus the magma budget (White *et al.* 2001). However, this dismisses the importance of varying mantle source composition relative to temperature (Zhou & Dick 2013). At increasingly slower spreading rates and lower extents of melting, more fertile mantle heterogeneities are sampled preferentially which may lead to greater crustal thickness variations for ultraslow-spreading ridges and thus also to greater variation in surface roughness. On the lower end of the roughness spectra, short wave heterogeneities in the back-arc mantle of the North-Fiji basin has been inferred to explain the segmentation of the SPR (Garel *et al.* 2003). There, the low roughness may be partly explained by a smooth seafloor resulting mainly from the coalescence of numerous volcanoes (Lagabrielle *et al.* 1996; Garel *et al.* 2003). On the Sheba ridge, the western area appears to be affected by excess magmatism (Leroy *et al.* 2010a) that may explain the very low roughness values there. Although error bars on crustal thickness are large, this tendency for increasing roughness when crustal thickness decreases makes sense as thinner magmatic crust, hence a greater mantle component in the lithosphere, would imply greater lithospheric strength. Roughness values larger than ~300 m may thus be characteristic of magma-poor sections of ultraslow-spreading ridges.

This tendency for higher roughness values in thinner crust areas is further complicated by the fact that the mean roughness value

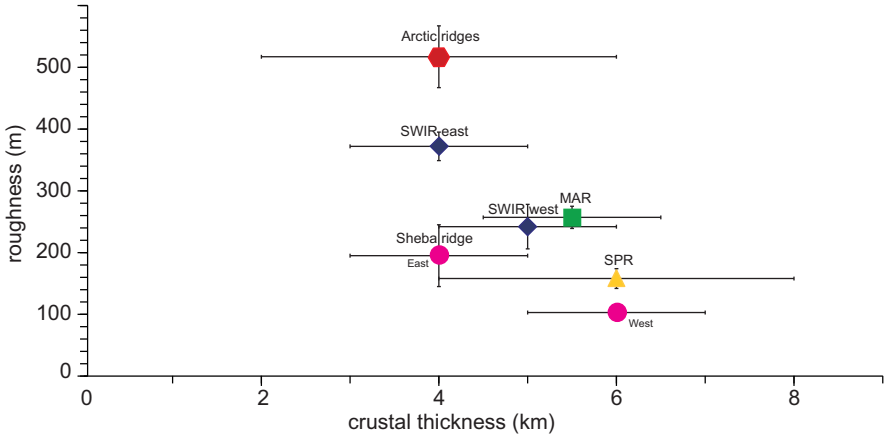

Figure 5. Roughness versus thickness of the magmatic crust for ultraslow-spreading ridges. Crustal thicknesses for the SWIR are from Cannat *et al.* (2008), those for the Sheba ridge are from d'Acremont *et al.* (2010), the one for the MAR is from Lizarralde *et al.* (2004), the one from the Arctic ridges is from Jokat & Schmidt-Aursch (2007) and Ehlers & Jokat (2009), the one for the SPR is from Garel *et al.* (2003).

for exhumed mantle domains at the SWIR is slightly lower (304 m) than for adjacent magmatic crust areas (372 m; Sloan *et al.* 2012). This is not expected as lithosphere should be thinner and weaker where magma supply is large and focused toward volcanic segment centres, and thicker and stronger where the magma supply is reduced or nearly absent (Cannat 1996). This apparent contradiction may be explained by considering the differences in both rheology and tectonic deformation style of magmatic segments and exhumed mantle domains. Within the magmatic segments, the volcanic seafloor composition is inferred to include the full complement of oceanic lithosphere components (i.e. volcanic and intrusive magmatic rocks overlying upper mantle) that tend to accommodate extension by high-angle normal faults. By contrast, the exhumed mantle domains are inferred to consist largely of serpentinized peridotites above unaltered mantle in which the formation of low-angle, long offset detachment faults is more common (Sauter *et al.* 2013). This is supported by the distribution of the seismicity between magmatic segment and exhumed mantle domains at ultraslow-spreading ridges. At the SWIR the magmatic segments, exhibit brittle deformation throughout the lithosphere up to 8–15 km depths in the upper mantle (Schlindwein & Schmid 2016). By contrast, although earthquakes are observed as deep as 35 km depths, the upper lithosphere is entirely aseismic up to 10 km depth along the adjacent peridotite-dominated ridge sections (Schmid & Schlindwein 2016). This observation of an upper aseismic zone has been interpreted as probably reflecting substantial serpentinization within the exhumed mantle domains of ultraslow-spreading ridges (Schmid & Schlindwein 2016).

The variation of oceanic basement roughness at ultraslow-spreading ridges is thus a complex trade-off between spreading rate that highly controls the thermal state of the lithosphere and its composition controlling the rheology and thus also the strength of the lithosphere.

5.2 Insight into the initial seafloor spreading

The roughness values determined over inferred initial oceanic domains are all higher than 200 m (Fig. 6), a typical value for slow-spreading ridges or magmatic sections of ultraslow-spreading ridges like the SPR or the Sheba Ridge (Fig. 4). Mean roughness values of the inferred initial oceanic domains bordering the Iberia and Newfoundland margins are greater than 300 m, which is characteristic of magma-poor sections of ultraslow-spreading ridges.

5.2.1 The Iberian/Newfoundland margin system

Roughness >500 m, as high as those found at the Arctic ridges (Ehlers & Jokat 2009), are found alongside the Iberia margin. There, oceanic domains with either thin crust or normal crustal thickness show high roughness values in the same way as along the Arctic ridges. Although significantly smaller than alongside the Iberia margin, roughness values alongside the Newfoundland margin are as large as those determined at the easternmost magma-poor SWIR. As these margins are conjugate, initial oceanic crust was emplaced at the same spreading centre and thus higher roughness values next to the Iberia margin cannot be explained by a lower spreading rate. Accretion may have been asymmetric with more detachment faulting eastward and more magmatic accretion westward as it is suggested on the MCSC (Hayman *et al.* 2011). However, there is no obvious difference between the basement morphologies in the inferred initial oceanic domains alongside the two margins. The overall different basement topography of the shallower Newfoundland margin compared to the deeper Iberia margin has been tentatively partly attributed to an 'inherited buoyancy' of the continental mantle at the Newfoundland margin (Müntener & Manatschal 2006). There, high degrees of melting formed a continental mantle lithosphere that might be compositionally buoyant (Müntener & Manatschal 2006). This hypothesis is consistent with the compositional differences between the Iberia and Newfoundland continental mantle derived peridotites (Müntener & Manatschal 2006). However, although the composition of the rising asthenospheric mantle is unknown, it is likely that its density structure is different from that of the adjacent continental mantle. A more homogenous density structure is rather expected below the two flanks of the initial oceanic ridge, which thus, could not explain a different strength of the initial oceanic lithosphere on the two margins. Alternatively, an explanation may be found in the widespread magmatism, which has been found in the distal domain of the Newfoundland margin (Péron-Pinvidic *et al.* 2010). There, by contrast to the Iberia margin, a major magmatic event, which post-dated the onset of seafloor spreading by at least 7–15 Myr (Hart & Blusztajn 2006), resulted in emplacement of sills over an area of ~80 000 km^2 above the exhumed mantle (Péron-Pinvidic *et al.* 2010). We therefore speculate that smoother initial

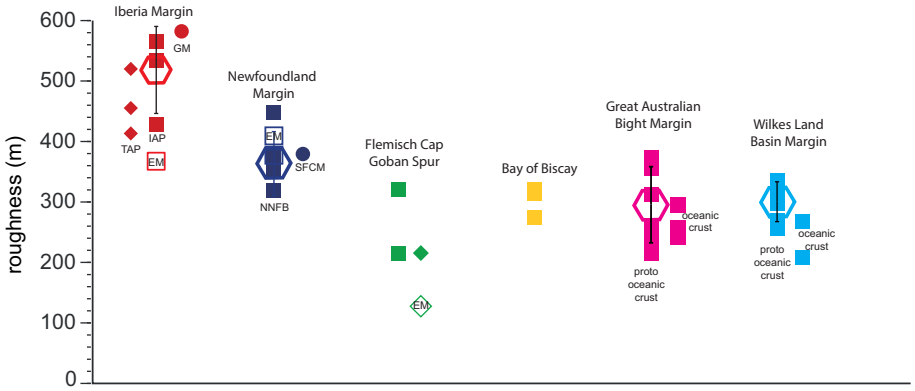

Figure 6. Roughness of initial oceanic basement alongside Iberia/Newfoundland, Flemish Cap/Goban Spur, Bay of Biscay, Australian Great Bight/Wilkes Land Basin margins. Open hexagons and vertical black lines correspond to the mean values and standard deviations, respectively, for each study area. EM: exhumed mantle. Roughness values and references are given in Table 2.

oceanic basement alongside the Newfoundland margin is related to the weakening of the initial oceanic lithosphere by this late magmatic event. The source of the magma is still uncertain and resolving this issue will require a combination of further geophysical studies and drilling (Péron-Pinvidic *et al.* 2010). Anyhow, we stress that initial oceanic crust alongside both margins exhibit roughness values on the higher end of the spectrum of ultraslow-spreading ridges regardless of the thickness of this initial oceanic crust. Although basement ridges display larger relief next to the Iberia margin, these ridges are on both margins generally symmetric, either with a domal or a triangular shape, without a clear oceanward faulting pattern that would characterize an oceanic magmatic crust with a normal thickness. Landward-dipping reflectors interpreted as faults are rather found on both the exhumed mantle domain of each margin and over the oceanic crust next to it (e.g. Welford *et al.* 2010b; Minshull *et al.* 2014). These structures were interpreted as abandoned fault roots resulting from successive mantle unroofing episodes (Boillot & Froitzheim 2001) as new detachments repeatedly cut through the footwall of the preceding detachment (Reston & McDermott 2011), a 'flip-flop' mechanism that has been later shown to be active at the ultraslow-spreading SWIR (Sauter *et al.* 2013).

5.2.2 The Flemish Cap/Goban Spur margin system

By contrast to the Iberia–Newfoundland margin, the top basement in the initial oceanic crust alongside the Flemish Cap and GS conjugate margins shows a tilted block morphology typical of slow-spreading ridges (Bullock & Minshull 2005; Gerlings *et al.* 2012). There, oceanward faults were identified in inferred oceanic domains displaying a 215 m roughness value, typical of slow-spreading ridges. A more irregular pattern of dome shaped ridges results in a rougher basement along the F87–3 line (322 m). Gerlings *et al.* (2012) already noted that the relief of the initial oceanic basement was rougher along the F87–3 line than on the conjugate GS line (216 m). They suggested that the initial igneous accretion was more dominant on Flemish Cap than on its conjugate. We rather argue that, although the velocity (5.8–7 km s^{-1}) of the lower crust at the inferred initial oceanic domain of GS is ambiguous and could support either a gabbroic or serpentinized composition, the roughness of the top basement, its morphology and the ∼6 km thickness of the inferred initial crust indicate typical slow seafloor spreading. The irregular pattern of dome shaped ridges along the F87–3 line may result from asymmetric spreading with oceanic core complex development westward while volcanism dominates eastward on the GS margin. Such asymmetry is often observed locally on slow-spreading ridges, close to transform faults, where magma supply is reduced relatively to the segment centres.

5.2.3 The Bay of Biscay margin system

Strong constraints are lacking to clearly determine the accretion processes that produced the initial oceanic domain in the BB. Roughness values are similar to some sections of the ultraslow-spreading SWIR, MCSC or MAR. The top basement is irregular showing either domes or symmetric ridges without tilted blocks typical of slow-spreading crust, which would indicate an ultraslow-spreading. However, compressional structures are observed in the sediment cover showing that some faults were slightly reactivated during the Iberian/European convergence (Thinon *et al.* 2001; Tugend *et al.* 2014). The extent of the resulting change of roughness and morphology is not yet constrained. Moreover, the crustal thickness is highly variable with overthickened crust in some places (Tugend *et al.* 2015). Therefore, we stress that more MCS data extending well into the inferred oceanic domain are needed to resolve the initial accretion processes in the BB.

5.2.4 The Australian Great Bight/Wilkes Land Basin margin system

Although there is some overlap between the ranges of roughness values, the mean values are significantly different for the proto-oceanic crust (296–300 m) and steady state oceanic crust (266–239 m) defined by (Gillard *et al.* 2015) at the Great Australian Bight and the Wilkes Land Basin, respectively (Table 2 and Fig. 6). Reflections that could correspond to the oceanic Moho are only locally observed below steady state oceanic crust, leading to a normal thickness (∼2 s TWTT) estimation. This oceanic domain was therefore rather defined by the highly reflective top basement on the MCS data and by the absence of deformation at the base of the sediment cover (Gillard *et al.* 2015). Roughness values of the steady state oceanic crust, only slightly larger than those typical of slow-spreading crust, are relatively low for ultraslow-spreading crust. As in the BB, the top basement is irregular without successive ridgeward facing faults typical of slow-spreading crust. By contrast, at both Australian and Antarctic margins, high structures associated with ridgeward-dipping intrabasement reflections were interpreted as oceanic core complexes produced by detachment faults (Gillard *et al.* 2015). Numerical models show that conditions of high or very low magma supply do not favour detachment faulting and that core

complexes occur with intermediate magma supply (Tucholke *et al.* 2008). We therefore argue that both the roughness and the morphology of the top basement indicate large tectonic extension and intermediate magma supply with either slow or ultraslow-spreading rate. We discuss the roughness of the proto-oceanic crust in the next section.

5.3 Proto versus initial oceanic basement

The proto-oceanic crust defined alongside the Australian and Antarctic margins is inferred to correspond to serpentinized peridotites that are intensively faulted and intruded (Gillard *et al.* 2016a). It differs from the exhumed mantle domain by oceanward increasing volcanic additions sealing the faulted top basement and intruding or underplating this basement (Gillard *et al.* 2016a). This type of hybrid crust with mantle derived rocks and magmatic rocks, might thus be similar to the exhumed mantle domains between initial oceanic crust and hyperextended continental crust at the Newfoundland-Iberia or Flemish Cap-GS margin systems. However, the amount of melt may be highly variable from one margin to the other or even along the margins themselves (Fig. 1). Roughness values are highly variable in both exhumed mantle domains and proto-oceanic crust ranging from low values (<130 m on GS margin (Bullock & Minshull 2005)) to very high values (>400 m on Newfoundland margin). This dispersion of the roughness values may result from variable extent of post rift volcanism, from highly intruded basement at the Australian and Antarctic margins resulting in a relatively rough seafloor, to a smoother exhumed mantle domain with little or no evidence for melting on GS margin (Bullock & Minshull 2005).

However, although the Iberia margin (including Galicia bank) is part of the magma-poor class of margins, the high roughness there is not produced by volcanic edifices but by high relief peridotite ridges inferred to result from successive faulting episodes (e.g. Reston & McDermott 2011). On the Newfoundland margin relatively smooth parts made of exhumed mantle are adjacent to much rougher basement. There, the prominent peridotite ridge drilled at ODP Site 1277 is thought to result from a significant tectonic uplift accompanied by a magmatic event that may have triggered the onset of seafloor spreading (Bronner *et al.* 2011). This illustrates the fundamental difference in nature between proto-oceanic crust or exhumed mantle domain and steady state oceanic crust. While deformation and magmatism are localized at oceanic ridges, multiple tectonic and magmatic episodes may have affected the whole proto-oceanic/exhumed mantle domains leading to highly variable top basement roughness.

6 FURTHER IMPLICATIONS

The underlying issue of the determination of the spreading rate at nascent spreading centres is to understand if there, the accretion processes are somehow related to the processes of lithospheric breakup. If spreading is ultraslow alongside every magma-poor rifted margins it could be tempting to suggest that the ultraslow-spreading rate is a consequence of the breakup processes at magma-poor rifted margins. However, among the examples analysed in this paper, only the Iberia–Newfoundland margin system shows clear evidence for initial ultraslow oceanic spreading. Disputable magnetic anomalies cannot be used to estimate the spreading rate alongside these margins and corroborate this result (Barnett-Moore *et al.* 2016; Nirrengarten *et al.* 2017). However, a new palinspastic restoration of the southern North-Atlantic based on 3D gravity inversion, which does not take into account disputed magnetic anomalies but which integrates the rift deformation (Sutra *et al.* 2013), allows to estimate the initial spreading rate alongside these margins (Nirrengarten *et al.* submitted). Ultraslow-spreading rates <17 mm yr^{-1} were obtained between 112 and 87Ma at the onset of accretion before reaching slow-spreading rate (>22 mm yr^{-1}; Nirrengarten *et al.* submitted). This early evolution of the spreading rate between Iberia and Newfoundland is related to the motion of Iberia at that time, resulting in the propagation of seafloor spreading in the BB. When spreading stopped in the BB during Santonian time, oceanic spreading was no more distributed along three branches of a triple junction but became focused at the mid-Atlantic ridge. We therefore suggest that similarly to present day oceanic ridges, spreading at the initial oceanic ridge between Iberia and Newfoundland is controlled by global plate tectonics and is not related to the rifting processes leading to the final breakup.

7 CONCLUSIONS

The investigation of the top basement roughness at ultraslow-spreading ridges and within the inferred initial oceanic domain alongside magma-poor rifted margins leads to the following conclusions.

(1) The mean roughness values obtained at ultraslow-spreading ridges range from 100 to >500 m and includes 200–240 m roughness values which are typical of slow-spreading ridges.

(2) There is a weak tendency for increasing roughness at ultraslow-spreading ridges when magmatic crustal thickness decreases. This is related to the rheology of the oceanic lithosphere; a thinner magmatic crust, hence a greater mantle component in the lithosphere, implying greater lithospheric strength. Roughness values larger than ~300 m may be characteristic of magma-poor sections of ultraslow-spreading ridges.

(3) The top basement roughness values determined within the inferred initial oceanic domain alongside magma-poor rifted margins are all higher than 200 m, a typical value for slow-spreading ridges or magmatic sections of ultraslow-spreading ridges

(4) Mean roughness values of the inferred initial oceanic domains alongside the Iberia and Newfoundland margins are greater than 300 m which is characteristic of magma-poor sections of ultraslow-spreading ridges.

(5) The top basement in the initial oceanic crust alongside the Flemish Cap and GS margins shows roughness values and a tilted block morphology typical of slow-spreading ridges.

(6) Roughness values of the initial oceanic crust alongside the Australian-Antarctic margins are only slighter larger than those typical of slow-spreading crust. We suggest that the roughness and the morphology of the top basement along those margins indicate large tectonic extension and intermediate magma supply with either slow or ultraslow-spreading rate.

(7) Estimating roughness values within proto oceanic crust or exhumed mantle domains is less pertinent as polyphased tectonism and magmatism may have affected these domains leading to highly variable top basement roughness values that cannot be linked to a single monophase processes.

ACKNOWLEDGEMENTS

We acknowledge funding by 'Actions Marges' a TOTAL/INSU/IFP/IFREMER/BRGM program to DS and JA, and funding from

Modelling of Margins Phase 3 and 4 consortium for JT. We thank Ségolène Vitoux, Elena Metz and Hugo Ketterer for their work that led to this paper. We also gratefully acknowledge the two anonymous reviewer and the Editor, Donna Blackman, for their review and helpful comments.

REFERENCES

Afilhado, A., Matias, L., Shiobara, H., Hirn, A., Mendes-Victor, L. & Shimamura, H., 2008. From unthinned continent to ocean: the deep structure of the West Iberia passive continental margin at 38°N, *Tectonophysics,* **458,** 9–50.

Alvarez-Marron, J., Rubio, E. & Torne, M., 1997. Subduction-related structures in the North Iberian Margin, *J. geophys. Res.,* **102,** 22 497–22 511.

Amante, C. & Eakins, B.W., 2009. ETOPO1 1 Arc-minute global relief model: procedures, data sources and analysis, in *NOAA Technical Memorandum NESDIS NGDC-24*, ed. NOAA, National Geophysical Data Center.

Ball, P.J., 2005. Break-up history and evolution of the southern passive margin of Australia, *PhD thesis*, Royal Holloway University, London.

Barnett-Moore, N., Hosseinpour, M. & Maus, S., 2016. Assessing discrepancies between previous plate kinematic models of Mesozoic Iberia and their constraints, *Tectonics,* **35,** 1843–1862.

Beslier, M.O., 1996. Seismic Line LG12 in the Iberia Abyssal Plain, in *Iberia Abyssal Plain*, pp. 737–739, eds Whitmarsh, R.B., Sawyer, D.S., Klaus, A. & Masson, D.G., Ocean Drilling Program.

Beslier, M.O., Cornen, G. & Girardeau, J., 1996. Tectono-metamorphic evolution of peridotites from the ocean/continent transition of the Iberia Abyssal Plain margin, in *Proc. ODP, Sci. Results*, pp. 397–412, eds Whitmarsh, R.B., Sawyer, D.S., Klaus, A. & Masson, D.G., Ocean Drilling Program.

Boillot, G. & Froitzheim, N., 2001. Non-volcanic rifted margins, continental break-up and the onset of sea-floor spreading: some outstanding questions, *Geol. Soc., London, Spec. Publ.,* **187,** 9–30

Bronner, A., Sauter, D., Manatschal, G., Peron-Pinvidic, G. & Munschy, M., 2011. Magmatic breakup as an explanation for magnetic anomalies at magma-poor rifted margins, *Nat. Geosci.,* **4,** 549–553.

Bullock, A.D. & Minshull, T.A., 2005. From continental extension to seafloor spreading: crustal structure of the Goban Spur rifted margin, southwest of the UK, *Geophys. J. Int.,* **163,** 527–546.

Cannat, M., 1993. Emplacement of mantle rocks in the seafloor at mid-ocean ridges, *J. geophys. Res.,* **98,** 4163–4172.

Cannat, M., 1996. How thick is the magmatic crust at slow spreading oceanic ridges?, *J. geophys. Res.,* **101,** 2847–2857.

Cannat, M., Sauter, D., Mendel, V., Ruellan, E., Okino, K., Escartin, J., Combier, V. & Baala, M., 2006. Modes of seafloor generation at a melt-poor ultraslow-spreading ridge, *Geology,* **34,** 605–608.

Cannat, M., Sauter, D., Bezos, A., Meyzen, C., Humler, E. & Le Rigoleur, M., 2008. Spreading rate, spreading obliquity, and melt supply at the ultraslow spreading Southwest Indian Ridge, *Geochem. Geophys. Geosyst.,* **9**, Q04002, doi:10.1029/2007GC001676.

Cannat, M., Manatschal, G., Sauter, D. & Peron-Pinvidic, G., 2009. Assessing the conditions of continental breakup at magma-poor rifted margins: What can we learn from slow spreading mid-ocean ridges?, *C. R. Geosci.,* **341,** 406–427

Chen, Y. & Morgan, W.J., 1990. Rift valley/no rift valley transition at mid-ocean ridges, *J. geophys. Res.,* **95,** 17 571–17 581.

Cunha, T., 2008. Gravity Anomalies, Flexure and the Thermo-Mechanical Evolution of the West Iberia Margin and its Conjugate of Newfoundland, *PhD thesis*, University of Oxford, Oxford.

D'Acremont, E., Leroy, S., Maia, M., Gente, P. & Autin, J., 2010. Volcanism, jump and propagation on the Sheba ridge, eastern Gulf of Aden: segmentation evolution and implications for oceanic accretion processes, *Geophys. J. Int.,* **180,** 535–551.

Davy, R.G. *et al.*, 2016. Continental hyperextension, mantle exhumation and thin oceanic crust at the continent-ocean transition, West Iberia: new insights from wide-angle seismic, *J. geophys. Res.,* **121,** 3177–3199.

Dean, S.M., Minshull, T.A., Whitmarsh, R.B. & Louden, K.E., 2000. Deep structure of the ocean-continent transition in the southern Iberia Abyssal Plain from seismic refraction profiles: The IAM-9 transect at 40°20′N, *J. geophys. Res.,* **105,** 5859–5885.

Dean, S.L., Sawyer, D.S. & Morgan, J.K., 2015. Galicia Bank ocean–continent transition zone: New seismic reflection constraints, *Earth planet. Sci. Lett.,* **413,** 197–207.

Delescluse, M., Funck, T., Dehler, S.A., Louden, K.E. & Watremez, L., 2015. The oceanic crustal structure at the extinct, slow to ultra-slow Labrador Sea spreading center, *J. geophys. Res.,* **120,** 5249–5272.

Dick, H.J.B., Lin, J. & Schouten, H., 2003. An ultraslow-spreading class of ocean ridge, *Nature,* **426,** 405–412.

Ehlers, B. & Jokat, W., 2009. Subsidence and crustal roughness of ultra-slow spreading ridges in the northern North Atlantic and the Arctic Ocean, *Geophys. J. Int.,* **177,** 451–462.

Fernández-Viejo, G., Gallart, J., Pulgar, J.A., Gallastegui, J., Dañobeitia, J.J. & Córdoba, D., 1998. Crustal transition between continental and oceanic domains along the North Iberian Margin from wide angle seismic and gravity data, *Geophys. Res. Lett.,* **25,** 4249–4252.

Fernández-Viejo, G., Pulgar, J.A., Gallastegui, J. & Quintana, L., 2012. The fossil accretionary wedge of the Bay of Biscay: critical wedge analysis on depth-migrated seismic sections and geodynamical implications, *J. Geol.,* **120,** 315–331.

Fournier, M., Patriat, P. & Leroy, S., 2001. Reappraisal of the Arabia–India–Somalia triple junction kinematics, *Earth planet. Sci. Lett.,* **189,** 103–114.

Funck, T., Hopper, J.R., Larsen, H.C., Louden, K.E., Tucholke, B.E. & Holbrook, W.S., 2003. Crustal structure of the ocean-continent transition at Flemish Cap: seismic refraction results, *J. geophys. Res.,* **108**(B11), 2531, doi:10.1029/2003JB002434.

Garel, E., Lagabrielle, Y. & Pelletier, B., 2003. Abrupt axial variations along the slow to ultra-slow spreading centers of the northern North Fiji Basin (SW Pacific): Evidence for short wave heterogeneities in a back-arc mantle, *Mar. Geophys. Res.,* **24,** 245–263.

Gerlings, J., Louden, K.E. & Jackson, H.R., 2011. Crustal structure of the Flemish Cap Continental Margin (eastern Canada): an analysis of a seismic refraction profile, *Geophys. J. Int.,* **185,** 30–48.

Gerlings, J., Louden, K.E., Minshull, T.A. & Nedimovic, M.R., 2012. Flemish Cap-Goban Spur conjugate margins: New evidence of asymmetry, *Geology,* **40,** 1107–1110.

Gillard, M., 2014. Évolution tectono-magmatique menant à l'océanisation sur les marges passives pauvres en magma, exemple des marges Australie-Antarctique, *PhD thesis*, University of Strasbourg, Strasbourg.

Gillard, M., Autin, J., Manatschal, G., Sauter, D., Munschy, M. & Schaming, M., 2015. Tectonomagmatic evolution of the final stages of rifting along the deep conjugate Australian-Antarctic magma-poor rifted margins: constraints from seismic observations, *Tectonics,* **34,** 753–783.

Gillard, M., Autin, J. & Manatschal, G., 2016a. Fault systems at hyper-extended rifted margins and embryonic oceanic crust: Structural style, evolution and relation to magma, *Mar. Pet. Geol.,* **76,** 51–67.

Gillard, M., Manatschal, G. & Autin, J., 2016b. How can asymmetric detachment faults generate symmetric ocean continent transitions?, *Terra Nova,* **28,** 27–34.

Goff, J.A., 1991. A Global and Regional Stochastic Analysis of Near-Ridge Abyssal Hill Morphology, *J. geophys. Res.,* **96,** 21 713–21 737.

Goff, J.A. & Jordan, T.H., 1988. Stochastic modeling of seafloor morphology: inversion of sea beam data for second-order statistics, *J. geophys. Res.,* **93,** 13 589–13 608.

Goff, J.A. & Jordan, T.H., 1989. Stochastic modeling of seafloor morphology; Resolution of topographic parameters by sea beam data, *IEEE J. Ocean. Eng.,* **14,** 326–337.

Goff, J.A., Tucholke, B.E., Lin, J., Jaroslow, G.E. & Kleinrock, M.C., 1995. Quantitative analysis of abyssal hills in the Atlantic Ocean: A correlation between inferred crustal thickness and extensional faulting, *J. geophys. Res.,* **100,** 22 509–22 522.

Goff, J.A., Ma, Y., Shah, A., Cochran, J.R. & Sempéré, J., 1997. Stochastic analysis of seafloor morphology on the flank of the Southeast Indian Ridge: The influence of ridge morphology on the formation of abyssal hills, *J. geophys. Res.,* **102,** 15 521–15 534.

Hart, S. & Blusztajn, J., 2006. Age and geochemistry of the mafic sills, ODP site 1276, Newfoundland margin, *Chem. Geol.,* **235,** 222–237.

Haupert, I., Manatschal, G., Decarlis, A. & Unternehr, P., 2016. Upper-plate magma-poor rifted margins: Stratigraphic architecture and structural evolution, *Mar. Pet. Geol.,* **69,** 241–261.

Hayman, N.W., Grindlay, N.R., Perfit, M.R., Mann, P., Leroy, S. & De Lépinay, B.M., 2011. Oceanic core complex development at the ultraslow spreading Mid-Cayman Spreading Center, *Geochem. Geophys. Geosyst.,* **12**.

Hopper, J.R., Funck, T., Tucholke, B.E., Christian Larsen, H., Holbrook, W.S., Louden, K.E., Shillington, D. & Lau, H., 2004. Continental breakup and the onset of ultraslow seafloor spreading off Flemish Cap on the Newfoundland rifted margin, *Geology,* **32,** 93–96.

Jagoutz, O., Muntener, O., Manatschal, G., Rubatto, D., Peron-Pinvidic, G., Turrin, B.D. & Villa, I.M., 2007. The rift-to-drift transition in the North Atlantic: a stuttering start of the MORB machine?, *Geology,* **35,** 1087–1090.

Jokat, W. & Schmidt-Aursch, M.C., 2007. Geophysical characteristics of the ultraslow spreading Gakkel Ridge, Arctic Ocean, *Geophys. J. Int.,* **168,** 983–998.

Jokat, W., Ritzmann, O., Schmidt-Aursch, M.C., Drachev, S., Gauger, S. & Snow, J., 2003. Geophysical evidence for reduced melt production on the Arctic ultraslow Gakkel mid-ocean ridge, *Nature,* **423,** 962–965.

Klimke, J., Franke, D., Gaedicke, C., Schreckenberger, B., Schnabel, M., Stollhofen, H., Rose, J. & Chaheire, M., 2016. How to identify oceanic crust—Evidence for a complex break-up in the Mozambique Channel, off East Africa, *Tectonophysics,* **693,** 436–452.

Lagabrielle, Y. *et al.*, 1996. Active oceanic spreading in the northern North Fiji Basin: Results of the NOFI cruise of R/V L'Atalante (newstarmer project), *Mar. Geophys. Res.,* **18,** 225–247.

Leroy, S., Mercier de Lepinay, B., Mauffret, A. & Pubellier, M., 1996. Structural and tectonic evolution of the eastern Cayman Trough (Caribbean Sea) from seismic reflection data, *AAPG Bull.,* **80,** 222–247.

Leroy, S., Mauffret, A., Patriat, P. & Mercier De Lepinay, B., 2000. An alternative interpretation of the Cayman trough evolution from a reidentification of magnetic anomalies, *Geophys. J. Int.,* **141,** 539–557.

Leroy, S. *et al.*, 2004. From rifting to spreading in the eastern Gulf of Aden: a geophysical survey of a young oceanic basin from margin to margin, *Terra Nova,* **16,** 185–192.

Leroy, S., D'acremont, E., Tiberi, C., Basuyau, C., Autin, J., Lucazeau, F. & Sloan, H., 2010a. Recent off-axis volcanism in the eastern Gulf of Aden: Implications for plume–ridge interaction, *Earth planet. Sci. Lett.,* **293,** 140–153.

Leroy, S. *et al.*, 2010b. Contrasted styles of rifting in the eastern Gulf of Aden: A combined wide-angle, multichannel seismic, and heat flow survey, *Geochem. Geophys. Geosyst.,* **11**.

Li, J. *et al.*, 2015. Seismic observation of an extremely magmatic accretion at the ultraslow spreading Southwest Indian Ridge, *Geophys. Res. Lett.,* **42,** 2656–2663.

Lizarralde, D., Gaherty, J.B., Collins, J.A., Hirth, G. & Kim, S.D., 2004. Spreading-rate dependence of melt extraction at mid-ocean ridges from mantle seismic refraction data, *Nature,* **432,** 744–747.

Malinverno, A., 1991. Inverse square-root dependence of mid-ocean-ridge flank roughness on spreading rate, *Nature,* **352,** 58–60.

Mcdermott, K. & Reston, T., 2015. To see, or not to see? Rifted margin extension, *Geology,* **43,** 967–970.

Mendel, V., Sauter, D., Rommevaux-Jestin, C., Patriat, P., Lefebvre, F. & Parson, L.M., 2003. Magmato-tectonic cyclicity at the ultra-slow spreading Southwest Indian Ridge: evidence from variations of axial volcanic ridge morphology and abyssal hills pattern, *Geochem. Geophys. Geosyst.,* **4,** doi:9110.1029/2002GC000417.

Michael, P.J. *et al.*, 2003. Magmatic and amagmatic seafloor generation at the ultraslow-spreading Gakkel ridge, Arctic Ocean, *Nature,* **423,** 956–961.

Minshull, T.A., 1999. On the roughness of Mesozoic oceanic crust in the western North Atlantic, *Geophys. J. Int.,* **136,** 286–290.

Minshull, T.A., 2009. Geophysical characterisation of the ocean–continent transition at magma-poor rifted margins, *C. R. Geosci.,* **341,** 382–393

Minshull, T.A., Muller, M.R. & White, R.S., 2006. Crustal structure of the Southwest Indian Ridge at 66°E: seismic constraints, *Geophys. J. Int.,* **166,** 135–147.

Minshull, T.A., Dean, S.M. & Whitmarsh, R.B., 2014. The peridotite ridge province in the southern Iberia Abyssal Plain: seismic constraints revisited, *J. geophys. Res.,* **119,** 1580–1598.

Muller, M.R., Minshull, T.A. & White, R.S., 1999. Segmentation and melt supply at the Southwest Indian Ridge, *Geology,* **27,** 867–870.

Müntener, O. & Manatschal, G., 2006. High degrees of melt extraction recorded by spinel harzburgite of the Newfoundland margin: The role of inheritance and consequences for the evolution of the southern North Atlantic, *Earth planet. Sci. Lett.,* **252,** 437–452.

Neumann, G.A. & Forsyth, D.W., 1995. High resolution statistical estimation of seafloor morphology: Oblique and orthogonal fabric on the flanks of the Mid-Atlantic Ridge, 34°–35.5°S, *Mar. Geophys. Res.,* **17,** 221–250.

Nirrengarten, M., Manatschal, G., Tugend, J., Kusznir, N.J. & Sauter, D., 2017. Nature and origin of the J-magnetic anomaly offshore Iberia-Newfoundland: implications for plate reconstructions, *Terra Nova,* **29,** 20–28.

Nirrengarten, M., Manatschal, G., Tugend, J., Kusznir, N.J. & Sauter, D., submitted. Kinematic evolution of the southern North Atlantic: implications for the formation of hyper-extended rift systems, *Tectonics*.

Niu, X. *et al.*, 2015. Along-axis variation in crustal thickness at the ultraslow spreading Southwest Indian Ridge (50°E) from a wide-angle seismic experiment, *Geochem. Geophys. Geosyst.,* **16,** 468–485.

Patriat, P., Sloan, H. & Sauter, D., 2008. From slow to ultraslow: A previously undetected event at the Southwest Indian Ridge at ca. 24 Ma, *Geology,* **36,** 207–210.

Péron-Pinvidic, G., Shillington, D.J. & Tucholke, B.E., 2010. Characterization of sills associated with the U reflection on the Newfoundland margin: evidence for widespread early post-rift magmatism on a magma-poor rifted margin, *Geophys. J. Int.,* **182,** 113–136.

Peron-Pinvidic, G., Manatschal, G. & Osmundsen, P.T., 2013. Structural comparison of archetypal Atlantic rifted margins: A review of observations and concepts, *Mar. Pet. Geol.,* **43,** 21–47.

Phipps Morgan, J. & Chen, Y.J., 1993. Dependence of ridge-axis morphology on magma supply and spreading rate, *Nature,* **364,** 706–708.

Pickup, S.L.B., Whitmarsh, R.B., Fowler, C.M.R. & Reston, T.J., 1996. Insight into the nature of the ocean-continent transition off West Iberia from a deep multichannel seismic reflection profile, *Geology,* **24,** 1079–1082.

Ranero, C.R. & Perez-Gussinye, M., 2010. Sequential faulting explains the asymmetry and extension discrepancy of conjugate margins, *Nature,* **468,** 294–299.

Ranero, C.R., Banda, E. & Buhl, P., 1997. The crustal structure of the Canary Basin: accretion processes at slow spreading centers, *J. geophys. Res.,* **102,** 10185–10201.

Reid, I. & Jackson, H.R., 1981. Oceanic spreading rate and crustal thickness, *Mar. Geophys. Res.,* **5,** 165–172.

Reston, T.J. & Mcdermott, K.G., 2011. Successive detachment faults and mantle unroofing at magma-poor rifted margins, *Geology,* **39,** 1071–1074.

Sauter, D., Mendel, V., Rommevaux-Jestin, C., Parson, L.M., Fujimoto, H., Mével, C., Cannat, M. & Tamaki, K., 2004. Focused magmatism versus amagmatic spreading along the ultra-slow spreading southwest Indian ridge: evidence from TOBI side scan sonar imagery, *Geochem. Geophys. Geosyst.,* **5,** doi:10.1029/2004GC000738.

Sauter, D., Cannat, M., Meyzen, C., Bezos, A., Patriat, P., Humler, E. & Debayle, E., 2009. Propagation of a melting anomaly along the ultraslow Southwest Indian Ridge between 46°E and 52°20′E: interaction with the Crozet hotspot?, *Geophys. J. Int.,* **179,** 687–699.

Sauter, D., Sloan, H., Cannat, M., Goff, J., Patriat, P., Schaming, M. & Roest, W.R., 2011. From slow to ultra-slow: How does spreading rate affect seafloor roughness and crustal thickness?, *Geology,* **39,** 911–914.

Sauter, D. *et al.*, 2013. Continuous exhumation of mantle-derived rocks at the Southwest Indian Ridge for 11 million years, *Nat. Geosci.,* **6,** 314–320.

Sauter, D. *et al.*, 2016. Evidence for magma entrapment below oceanic crust from deep seismic reflections in the Western Somali Basin, *Geology,* **44,** 407–410.

Sayers, J., Symonds, P.A., Direen, N.G. & Bernardel, G., 2001. Nature of the continent-ocean transition on the non-volcanic rifted margin of the central Great Australian Bight, *Geol. Soc., London, Spec. Publ.,* **187,** 51–76.

Schlindwein, V. & Schmid, F., 2016. Mid-ocean-ridge seismicity reveals extreme types of ocean lithosphere, *Nature,* **535** 276–279.

Schmid, F. & Schlindwein, V., 2016. Microearthquake activity, lithospheric structure, and deformation modes at an amagmatic ultraslow spreading Southwest Indian Ridge segment, *Geochem. Geophys. Geosyst.,* **17,** 2905–2921.

Shaw, W.J. & Lin, J., 1996. Models of ocean ridge lithospheric deformation: Dependence on crustal thickness, spreading rate, and segmentation, *J. geophys. Res.,* **101,** 17 977–17 993.

Shillington, D.J. *et al.*, 2006. Evidence for asymmetric nonvolcanic rifting and slow incipient oceanic accretion from seismic reflection data on the Newfoundland margin, *J. geophys. Res.,* **111,** B09402, doi:10.1029/2005JB003981.

Sloan, H., Sauter, D., Goff, J.A. & Cannat, M., 2012. Abyssal hill characterization at the ultraslow spreading Southwest Indian Ridge, *Geochem. Geophys. Geosyst.,* **13**.

Small, C., 1994. A global analysis of mid-ocean ridge axial topography, *Geophys. J. Int.,* **116,** 64–84.

Stanton, N., Manatschal, G., Autin, J., Sauter, D., Maia, M. & Viana, A., 2016. Geophysical fingerprints of hyper-extended, exhumed and embryonic oceanic domains: the example from the Iberia–Newfoundland rifted margins, *Mar. Geophys. Res.,* **37,** 185–205.

Sundvik, M., Larson, R.L. & Detrick, R.S., 1984. Rough-smooth basement boundary in the western North Atlantic basin: evidence for a seafloor-spreading origin, *Geology,* **12,** 31–34.

Sutra, E. & Manatschal, G., 2012. How does the continental crust thin in a hyperextended rifted margin? Insights from the Iberia margin, *Geology,* **40,** 139–142.

Sutra, E., Manatschal, G., Mohn, G. & Unternehr, P., 2013. Quantification and restoration of extensional deformation along the Western Iberia and Newfoundland rifted margins, *Geochem. Geophys. Geosyst.,* **14,** 2575–2597.

Ten Brink, U.S., Coleman, D.F. & Dillon, W.P., 2002. The nature of the crust under Cayman Trough from gravity, *Mar. Pet. Geol.,* **19,** 971–987.

Thinon, I., Fidalgo-González, L., Réhault, J. & Olivet, J., 2001. Déformations pyrénéennes dans le golfe de Gascogne, *C. R. Acad. Sci., Paris II,* **332,** 561–568.

Thinon, I., Matias, L., Rehault, J.P., Hirn, A., Fidalgo-Gonzalez, L. & Avedik, F., 2003. Deep structure of the Armorican Basin (Bay of Biscay): a review of Norgasis seismic reflection and refraction data, *J. Geol. Soc.,* **160,** 99–116.

Tikku, A.A. & Cande, S.C., 1999. The oldest magnetic anomalies in the Australian-Antarctic Basin: Are they isochrons?, *J. geophys. Res.,* **104,** 661–677.

Tikku, A.A. & Direen, N.G., 2008. Comment on "Major Australian-Antarctic Plate Reorganization at Hawaiian-Emperor Bend Time", *Science,* **321,** 490.

Tucholke, B.E. & Sibuet, J.-C., 2007. Leg 210 synthesis: tectonic, magmatic, and sedimentary evolution of the Newfoundland-Iberia rift, in *Proceedings of the Ocean Drilling Program, Scientific Results*, pp. 1–56, eds Tucholke, B.E., Sibuet, J.-C. & Klaus, A., Ocean Drilling Program.

Tucholke, B.E., Behn, M.D., Buck, W.R. & Lin, J., 2008. Role of melt supply in oceanic detachment faulting and formation of megamullions, *Geology,* **36,** 455–458.

Tugend, J., Manatschal, G., Kusznir, N.J., Masini, E., Mohn, G. & Thinon, I., 2014. Formation and deformation of hyperextended rift systems: insights from rift domain mapping in the Bay of Biscay-Pyrenees, *Tectonics,* **33,** 1239–1276.

Tugend, J., Manatschal, G., Kusznir, N.J. & Masini, E., 2015. Characterizing and identifying structural domains at rifted continental margins: application to the Bay of Biscay margins and its Western Pyrenean fossil remnants, *Geol. Soc., London, Spec. Publ.,* **413,** 171–203.

Unternehr, P., Peron-Pinvidic, G., Manatschal, G. & Sutra, E., 2010. Hyperextended crust in the South Atlantic: in search of a model, *Pet. Geosci.,* **16,** 207–215.

Van Avendonk, H.J.A., Holbrook, W.S., Nunes, G.T., Shillington, D.J., Tucholke, B.E., Louden, K.E., Larsen, H.C. & Hopper, J.R., 2006. Seismic velocity structure of the rifted margin of the eastern Grand Banks of Newfoundland, Canada, *J. geophys. Res.,* **111,** B11404, doi:10.1029/2005JB004156.

Watremez, L., Leroy, S., Rouzo, S., D'acremont, E., Unternehr, P., Ebinger, C., Lucazeau, F. & Al-Lazki, A., 2011. The crustal structure of the northeastern Gulf of Aden continental margin: insights from wide-angle seismic data, *Geophys. J. Int.,* **184,** 575–594.

Weigelt, E. & Jokat, W., 2001. Peculiarities of roughness and thickness of oceanic crust in the Eurasian Basin, Arctic Ocean, *Geophys. J. Int.,* **145,** 505–516.

Welford, J.K., Hall, J., Sibuet, J. & Srivastava, S.P., 2010a. Structure across the northeastern margin of Flemish Cap, offshore Newfoundland from Erable multichannel seismic reflection profiles: evidence for a transtensional rifting environment, *Geophys. J. Int.,* **183,** 572–586.

Welford, J.K., Smith, J.A., Hall, J., Deemer, S., Srivastava, S.P. & Sibuet, J.-C., 2010b. Structure and rifting evolution of the northern Newfoundland Basin from Erable multichannel seismic reflection profiles across the southeastern margin of Flemish Cap, *Geophys. J. Int.,* **180,** 976–998.

White, R.S., Minshull, T.A., Bickle, M.J. & Robinson, C.J., 2001. Melt generation at very slow-spreading oceanic ridges: constraints from geochemical and geophysical data, *J. Pet.,* **42,** 1171–1196.

Whitmarsh, R.B., Manatschal, G. & Minshull, T.A., 2001. Evolution of magma-poor continental margins from rifting to seafloor spreading, *Nature,* **413,** 150–154.

Zhao, M. *et al.*, 2013. Three-dimensional seismic structure of the Dragon Flag oceanic core complex at the ultraslow spreading Southwest Indian Ridge (49°39′E), *Geochem. Geophys. Geosyst.,* **14,** 4544–4563.

Zhou, H. & Dick, H.J.B., 2013. Thin crust as evidence for depleted mantle supporting the Marion Rise, *Nature,* **494,** 195–200.